Dynamics of acetylene dimers hosted in helium droplets

M. Briant, E. Mengesha, M.-A. Gaveau, B. Soep, J.-M. Mestdagh, L. Poisson

PCCP

PAPER

View Article Online
View Journal | View Issue

Cite this: *Phys. Chem. Chem. Phys.*, 2018, **20**, 2597

Dynamics of acetylene dimers hosted in helium droplets

M. Briant, *[a] E. Mengesha,[ab] M.-A. Gaveau,[a] B. Soep,[a] J.-M. Mestdagh[a] and L. Poisson[a]

Received 16th November 2017,
Accepted 31st December 2017

DOI: 10.1039/c7cp07741f

rsc.li/pccp

The CH antisymmetric stretch of the C_2H_2 moieties in acetylene dimers was explored over the range 3270–3290 cm^{-1} using the helium nanodroplet isolation (HENDI) technique. This work is part of a general investigation which addresses the dynamical consequences of coupling the deformation motions of weakly bound complexes with a finite size quantum liquid (the helium droplet). The acetylene dimer is attractive from this point of view because one of its deformation coordinates promotes a tunneling isomerization process. A numerical simulation of the observed spectrum allows deriving a set of effective spectroscopic constants which help understanding the dynamical role played by the droplet on the rotation and deformation of the dimer.

1 Introduction

He-nanodroplets have a low enough temperature (0.38 K) to have a strong quantum character and be superfluid.[1] They appear to be ideal for hosting single molecules or a controlled number of molecules with minimal perturbation on their dynamics. In particular, this isolation technique, called helium nanodroplet isolation (HENDI), allows studying infrared spectroscopy of the hosted molecule(s) with rotational resolution.[2–6]

In spite of the superfluid character of the droplets, the rotation of hosted molecules is perturbed. A simple interpretation assumes that a non-superfluid helium component is developed about the hosted molecule. It is driven into rotation by a coupling with the rotation of the hosted molecule, which in turn is slowed down. An empirical description of this effect is to replace the rotational and centrifugal distortion constants of the free molecule by effective constants. This picture has been rationalized quantitatively on the grounds of path integral Monte Carlo calculations.[7–9]

Large amplitude bending deformations of a weakly bonded 1 : 1 atom–molecule (or molecule–molecule) complex can be considered as a rotation of the molecular moiety of the complex, hindered by the interaction with the other moiety. When the complex is hosted in a helium droplet, an issue is to explore the dynamical effect of the helium environment on the hindered rotation. Our group has initiated a general investigation of this issue. The Ne–C_2H_2 complex was explored first in a work which combines high resolution IR-HENDI-spectroscopy and numerical simulations.[10] The simulations are based on close-coupling calculations to derive the bound states of the Ne–C_2H_2 complex. Then, the dynamical effect of the helium environment is modeled phenomenologically in the same spirit as recalled above for molecular rotations. Effective values are given to the dynamical parameters that appear in the close-coupling calculation: the reduced mass of the Ne–C_2H_2 complex; the rotational and the centrifugal deformation constants of the C_2H_2 moiety.

A side results in ref. 10 concerns spectra where acetylene only is present in the droplet. Close to lines assigned to the low energy component of the $\nu_3/\nu_2 + \nu_4 + \nu_5$ Fermi dyad of the C_2H_2 monomer, bands assigned to the $K_a(2 \leftarrow 1)$, $K_a(1 \leftarrow 0)$ and $K_a(0 \leftarrow 1)$ transitions of the dimer $(C_2H_2)_2$ were observed. These assignments follow those of Nauta and Miller who reported the first HENDI experiment on the acetylene molecule.[11] The group of M. Havenith reported similar observations also.[12] In these works, the $(C_2H_2)_2$ data were considered as secondary and did not received attention beyond the assignments that are just recalled.

The present work complements the data of ref. 10. The issue of interest here is to unravel the perturbation brought by the droplet on the large amplitude movement of $(C_2H_2)_2$ along an interconversion tunneling coordinate, described in the next section, which exchanges the role of the two C_2H_2 units in $(C_2H_2)_2$. As in ref. 10, the present work combines high resolution IR-HENDI-spectroscopy and numerical simulations.

2 Current knowledge of the $(C_2H_2)_2$ structure and dynamics

The first observation of a free acetylene dimer was reported by Pendley and Ewing from a Fourier transform infrared

[a] *LIDYL, CEA, CNRS, Université Paris-Saclay, CEA Saclay, F-91191 Gif-sur-Yvette, France. E-mail: marc.briant@cea.fr*
[b] *College of Natural and Computational Science, Department of Chemistry, Haramaya University, P.O. Box 138, Dire Dawa, Ethiopia*

spectroscopy experiment.[13] Fraser *et al.* provided new experimental material using a pulsed-nozzle Fourier transform microwave spectrometer and reinterpreted infrared spectra of Prichard *et al.*[14] which documented the CH antisymmetric stretch of the C_2H_2 moieties in $(C_2H_2)_2$, close to the spectral region of the ν_3 transition in the C_2H_2 monomer.[15,16] These authors proposed a model recalled below and came to the conclusion, further confirmed experimentally[17–19] and theoretically,[20] that the ground vibrational dimer $(C_2H_2)_2$ has a T-shaped equilibrium structure where one of the H-atom of the C_2H_2 moieties is attracted by the π-electrons of the other moiety. To provide a picture of the complex, we follow Didriche *et al.*[19] We call body the C_2H_2 moiety which carries the bonded H-atom of the dimer and hat the other moiety (see Fig. 1). Importantly also, Fraser *et al.*[15] observed that the $\nu_3/\nu_2 + \nu_4 + \nu_5$ Fermi resonance which is active in the C_2H_2 monomer is quenched in the dimer.

Fraser *et al.*[15] and Ohshima *et al.*[17,18] proposed independently a description of the acetylene dimer which is grounded on the permutation-inversion group G_{16}. These authors assumed that the geared planar tunneling motion shown in Fig. 1, where the two C_2H_2 moieties perform a counter rotation by an angle α, is the minimum energy path which transforms the T-shaped dimer into isoenergetic T-shaped structures. Four isoenergetic minima are explored when α = 0, 90, 180 and 270°. Interconversion tunneling along this coordinate lifts the degeneracy. According to the state labeling in the G_{16} group, three tunneling states of symmetry A_1^+, E^+ (doubly degenerated) and B_1^+, are expected in order of increasing energies (see eqn (2)–(4) and Table III in ref. 15).

This 1D picture of the interconversion tunneling, although approximate, is consistent with the recent *ab initio* calculation of the acetylene dimer potential energy surface by Leforestier *et al.*[20] The latter calculation shows indeed that the out-of-plane motion of one acetylene moiety with respect to the other is blocked by a barrier of 483.6 cm^{-1} and that the geared motion of the two acetylene moieties goes through a much lower barrier of 49.9 cm^{-1}. The latter barrier is fully consistent with that of 33.2 cm^{-1} provided by the experimental work of Fraser *et al.*[15] The reason for the large value of the out-of-plane barrier is that the H-bond has to be broken to allow this movement.

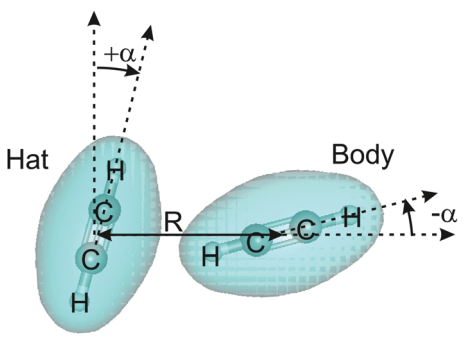

Fig. 1 Electronic density (90% from a simple RHF/pVDZ calculation) of the (C_2H_2) dimer. The equilibrium distance R = 4.36 Å between the acetylene moieties is taken from ref. 20. The angle α shows the counter rotation of the acetylene moieties when the dimer tunnels from one isomer to the other. The dimer is T-shaped at equilibrium. Isoenergetic equilibrium isomers are met when α = 0, 90, 180 and 270°.

When treating of the CH antisymmetric stretch excitation either in the body or the hat of the dimer, Fraser derived a simple model which couples excited potential curves along the tunneling coordinate α mentioned above.[16]

Finally, Didriche *et al.* showed that to predict the rovibrational spectroscopy of $(C_2H_2)_2$, it is possible to describe $(C_2H_2)_2$ as a semi-rigid asymmetric top molecule, provided effective ro-vibrational constants are given to each tunneling state.[19] The present work follows this procedure when simulating spectra.

3 Experiment

3.1 Experimental set-up

The experimental setup has been described already.[10] It was designed to perform rovibrational spectroscopy of species hosted in helium droplets, using the HENDI technique.

Briefly, a molecular beam source generates a beam carrying helium droplets with an average size of a few thousands helium atoms. The beam is passing through a pickup cell filled with C_2H_2. Varying the C_2H_2 pressure in this chamber allows varying the average number of C_2H_2 molecules which are deposited per droplet. Owing to the large binding energy of the dimer (548 cm^{-1})[20] compared to the droplet temperature (0.38 K ≡ 0.26 cm^{-1}) and the He–He potential well (0.75 cm^{-1}),[21] two C_2H_2 molecules, which are present on the same droplet, are bound together and form a dimer. Then, the beam crosses a tunable infrared optical parametric oscillator laser in a multipass mirror assembly. In the present experiment, the laser is scanned near 3.0 μm, between 3270 and 3290 cm^{-1}. When the laser frequency corresponds to a transition of the hosted species, the latter is excited. Since it is coupled to the droplet, the excitation energy is relaxed towards the droplet, which evaporates partially or totally. The corresponding decay of the droplet flux is monitored by recording the He_2^+ signal in a quadrupole mass spectrometer placed downstream the interaction region with the laser. The laser beam is chopped by a rotating disk. This allows using a lock-in amplifier to monitor the variations of the He_2^+ signal while scanning the laser.

3.2 Experimental spectrum and determination of the stoichiometry

The spectrum obtained by recording the depletion signal at mass He_2^+ as a function of the laser frequency is shown in Fig. 2. As we shall see below it contains information on droplets carrying either a single C_2H_2 molecule or a dimer.

The spectroscopy of the C_2H_2 monomer embedded in helium nanodroplets is well documented.[10–12] Because of the exchange property of the H-atoms (fermions of 1/2 nuclear spin), the C_2H_2 molecule exists under two forms: *para*-C_2H_2 (total nuclear spin I = 0; rotational levels of even quantum number J) and *ortho*-C_2H_2 (I = 1; odd J). The *ortho–para* exchange is nuclear-spin forbidden. Hence, although the droplet is very cold, 0.38 K, the J = 0 (*para*-C_2H_2) and J = 1 (*ortho*-C_2H_2) rotational levels of C_2H_2 are populated at the 1 : 3 ratio given by the nuclear spin statistics. Hence, P(1), R(0) and R(1) transitions are expected in

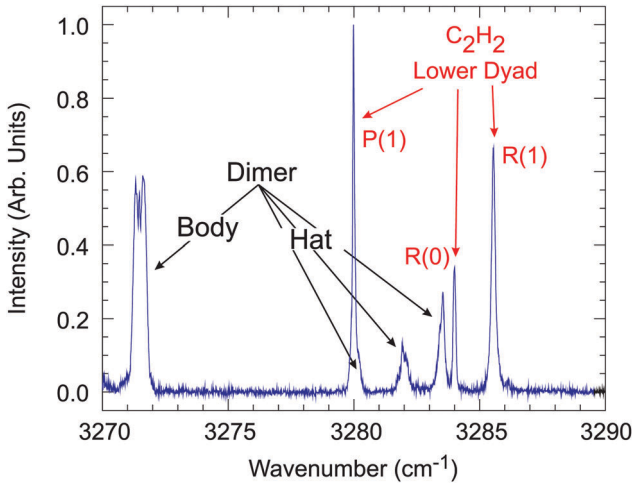

Fig. 2 Absorption spectrum recorded between 3270 and 3290 cm^{-1} when the droplets carry 1.6 C_2H_2 molecules in average. The assignments which label the spectral bands are justified in the text.

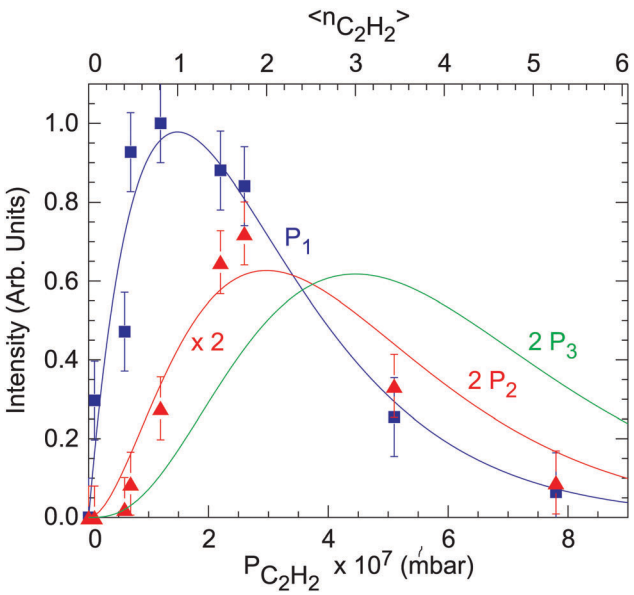

Fig. 3 Intensity of features observed in Fig. 2 as a function of the pick-up pressure $P_{C_2H_2}$ (bottom scale). The blue squares show the summed intensities of the lines labeled P(1), R(0) and R(1) and assigned to C_2H_2 in the figure. The red triangles show the summed intensities of the bands labeled "Dimer". The intensity of these bands was multiplied by 2 to avoid an accidental superimposition with blue squares at large pressures. The solid lines show the Poisson distributions P_1, $2 \times P_2$ and $2 \times P_3$ as labeled in the figure. The top and bottom scales were corresponded for the monomer data (blue squares) are best fitted by the first order Poisson distribution P_1.

each component of the $\nu_3/\nu_2 + \nu_4 + \nu_5$ Fermi dyad. Those corresponding to the low energy component of the dyad appear in Fig. 2 and are labeled accordingly (red labels).

Four bands are observed in Fig. 2 besides the C_2H_2 lines. They are assigned below to the $(C_2H_2)_2$ dimer and are labeled dimer in the figure. Note that one of them is almost hidden in the blue side of the C_2H_2 P(1) line.

The pick-up technique used to deposit C_2H_2 molecules on the droplets is a stochastic process. If neglecting helium atom evaporation after a C_2H_2 molecule has been captured, the pick-up has no memory between successive captures and is described by a Poisson statistics.[22] Hence, the signal which is attributed to the C_2H_2 monomer in Fig. 2 must follow the first order Poisson law P_1 when varying the C_2H_2 pressure $P_{C_2H_2}$ in the pick-up chamber.[23] This is shown in Fig. 3. The blue squares display the summed intensities of the P(1), R(0) and R(1) lines of C_2H_2 as a function of $P_{C_2H_2}$ and the blue curve the first order Poisson law $P_1(\langle n_{C_2H_2}\rangle) = \langle n_{C_2H_2}\rangle \exp(-\langle n_{C_2H_2}\rangle)$ which best fits the experimental data. The fit was performed by adjusting the proportionality factor between the average number $\langle n_{C_2H_2}\rangle$ of C_2H_2 molecules per droplet and the $P_{C_2H_2}$ pressure. The best fit was obtained with the correspondence shown in Fig. 3 between the upper scale ($\langle n_{C_2H_2}\rangle$) and the lower one ($P_{C_2H_2}$). In the same figure, the red triangles display the summed intensity of the bands that are observed in Fig. 2 besides the monomer lines. They are adequately fitted by the second order Poisson law $P_2(\langle n_{C_2H_2}\rangle) = \frac{1}{2!}\langle n_{C_2H_2}\rangle^2 \exp(-\langle n_{C_2H_2}\rangle)$. As a result, these lines are assigned to absorption of $(C_2H_2)_2$ and are labeled "Dimer" in Fig. 2.

4 Numerical simulation of the experimental spectrum

According to the correspondence above between $P_{C_2H_2}$ and $\langle n_{C_2H_2}\rangle$, we know that the spectrum reported in Fig. 2 was recorded with helium droplets carrying an average of 1.6 C_2H_2 molecules. Hence, 20% of the droplets in this experiment carry no C_2H_2 molecule, 32% a single molecule, 26% two molecules and the remaining 22% more than two molecules. The latter droplets do not need to be considered here since the absorption bands of the $(C_2H_2)_{>2}$ multimers fall outside the range covered in Fig. 2, 3265.3 cm^{-1} for $(C_2H_2)_3$ and 3261.1–3259.5 cm^{-1} for $(C_2H_2)_{\geq 4}$.[12] Hence, the spectrum shown in Fig. 2 is the superposition of two spectra, originating from droplets carrying one or two C_2H_2 molecules. The simulation treats each case specifically.

4.1 Droplets carrying a C_2H_2 monomer

The same treatment and the same spectroscopic constants as those reported in ref. 10 are used here. Accordingly, the frequency of the 3 transitions assigned to C_2H_2 in Fig. 2 is determined using the constants listed in Table 1: ν_{LD}^{He} gives the excitation energy to the lower component of the $\nu_3/\nu_2 + \nu_4 + \nu_5$ Fermi dyad; B^{He} is the effective rotational constant and D^{He} the effective centrifugal distortion constant, both being assumed to be the same whether C_2H_2 is in the ground vibrational state or vibrationally excited. A width of 0.08 cm^{-1} is assumed for each transition.

4.2 Droplets carrying a $(C_2H_2)_2$ dimer

The considerations recalled in Section 2 served as guideline to simulate the spectrum due to droplets that carry the $(C_2H_2)_2$ dimer.

Table 1 Effective constants (in cm^{-1}) used to simulate the contribution of droplets carrying a single C_2H_2 molecule. B^{He} and D^{He} are the rotational and centrifugal distortion constants, ν_{LD}^{He} is the origin of the lower component of the $\nu_3/\nu_2 + \nu_4 + \nu_5$ Fermi dyad of C_2H_2. Taken from Briant *et al.*[10]

B^{He}	1.04
D^{He}	0.019
ν_{LD}^{He}	3281.99

First, Fraser *et al.*[15] observed no sign of a Fermi resonance between ν_3 and $\nu_2 + \nu_4 + \nu_5$ in the dimer. Hence, only the ν_3 asymmetric stretch which carries oscillator strength was considered here. Second, the 1D model was used to determine the relative energetics and oscillator strength of the ν_3 excitation of the 3 tunneling isomers of the $(C_2H_2)_2$ dimer.[15,16] Finally, we followed Didriche *et al.* and simulated the full absorption spectrum by summing semi-rigid rotor simulations performed for each tunneling isomer.[19]

The simulation is split in 3 steps. Step (i) determines the relative energy and wavefunctions of the tunneling isomers of the ground state dimer; step (ii) provides the same information when one of the C_2H_2 moieties of the dimer is excited to the ν_3 mode; step (iii) simulates the absorption spectrum of each tunneling isomer due to the transitions between the levels found at steps (i) and (ii).

Step (i) – Ground state dimer – the ground state dimer is described by transposing eqn (20a), (20b) and (20c) of ref. 16 to the present helium droplet environment. The Hamiltonian which describes the dimer along the tunneling coordinate α is written as follow in wavenumber units:

$$H = -\frac{b_{C_2H_2}}{2}\frac{d^2}{d\alpha^2} + \frac{V_4}{2}(1 - \cos 4\alpha). \quad (1)$$

where $b_{C_2H_2}$ is the rotational constant of C_2H_2 and $\frac{d^2}{d\alpha^2}$ the second derivative with respect to α. In this equation, the term $\frac{V_4}{2}(1 - \cos 4\alpha)$ tells that the tunneling coordinate α samples 4 equivalent T-shaped structures of the dimer when it switches from 0 to 90, 180 and 270°. Physically, V_4 represents the height of the barrier which exchanges the tunneling isomers. It is considered here to be an intrinsic property of the complex and is, therefore, not modified by the droplet environment. We thus keep it to the value of 33.2 cm^{-1} found experimentally in ref. 15 for the free dimer. The phenomenological adaptation of eqn (1) to the presence of helium carries on the kinetic energy term $-\frac{b_{C_2H_2}}{2}\frac{d^2}{d\alpha^2}$. It is done very simply by assigning an effective value $b_{C_2H_2}^{He}$ to the rotational constant $b_{C_2H_2}$.

As in ref. 15 and 16, the eigenvectors $|\phi_g\rangle$ of Hamiltonian H are expanded over the basis $\sqrt{\frac{1}{2\pi}}\exp(\imath m\alpha)$ where $m = 0, \pm1, \pm2, \pm3, \ldots$ The 1-D Schrödinger equation $H|\phi_g\rangle = E|\phi_g\rangle$ is solved by numerical diagonalization of H on this basis, using the "*numpy.linalg.eigh*" routine of the Python package.[24] Values of m up to $|m| = 26$ are considered. This quite large value insures convergence with a reasonable computation time. As in ref. 15 and 16, it is

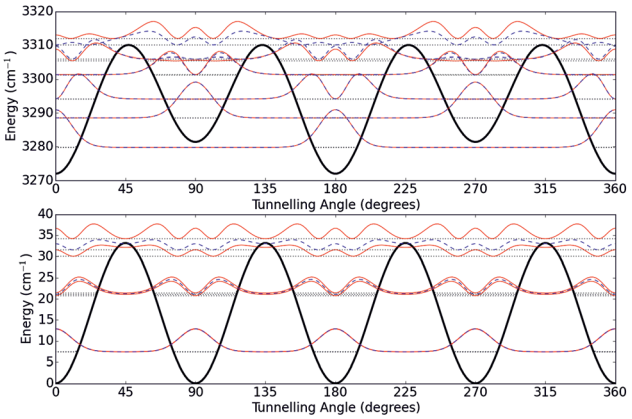

Fig. 4 Energy and wavefunctions of the lowest energy levels of the $(C_2H_2)_2$ dimer for deformations along the tunneling coordinate α whether the ν_3 asymmetric stretch is excited (top panel) or not (bottom panel). The calculation are performed using the tunneling barrier V_4, band origins ν_{hat} and ν_{body} and effective constant $b_{C_2H_2}^{He}$ listed in Table 2. The red (resp. blue) curves represent levels of A and B (resp. E) symmetry. The thin black lines shows the energy of these levels and the black heavy solid curves show the tunneling potential.

convenient to take into account the symmetry of the Hamiltonian by splitting the Hamiltonian matrix in two blocks whether m is even or odd. The former provides the tunneling states of A and B symmetries and the latter, the doubly degenerated E state. The bottom panel of Fig. 4 shows the energies and wavefunctions of the first three states in each symmetry along the tunneling coordinate α. These states, which describe the relative motion of the hat and body of the dimer along the tunneling coordinate can be considered also as reflecting hindered rotations of the hat and body within the droplet. Actually, it has been checked that the calculated states converge toward pure rotational states well above the tunneling barrier.

Step (ii) vibrationally excited dimer – in a similar way as just performed for the ground state, the vibrationally excited dimer is described by transposing the eqn (22a), (22b), (23a) and (23b) of ref. 16 to the context of a helium droplet. Eqn (1) is transformed as

$$\begin{aligned} H_a &= -\frac{b_{C_2H_2}}{2}\frac{d^2}{d\alpha^2} + \frac{V_4}{2}(1 - \cos 4\alpha) + hc\nu_{body} \\ &\quad + hc(\nu_{hat} - \nu_{body})\frac{(1 - \cos 2\alpha)}{2}, \end{aligned} \quad (2a)$$

$$\begin{aligned} H_b &= -\frac{b_{C_2H_2}}{2}\frac{d^2}{d\alpha^2} + \frac{V_4}{2}(1 - \cos 4\alpha) \\ &\quad + hc\nu_{hat} - hc(\nu_{hat} - \nu_{body})\frac{(1 - \cos 2\alpha)}{2}. \end{aligned} \quad (2b)$$

Two Hamiltonians, H_a and H_b, both written in wavenumber units, appear in eqn (2) because the excitation frequency is not the same whether the body (ν_{body}) or the hat (ν_{hat}) of the T-shaped dimer is excited. H_a (resp. H_b) corresponds to the body (resp. hat) excitation when $\alpha = 0°$. In these equations, the $(1 - \cos 2\alpha)$ factor assumes a smooth switch from the ν_{body}

to the ν_{hat} excitation when α is varied by 90°. Because of the $hc\nu_{body} + hc(\nu_{hat} - \nu_{body})\frac{(1-\cos 2\alpha)}{2}$ term in eqn (2a) (or the equivalent term in eqn (2b)), the interaction energy between the C_2H_2 moieties of the dimer in the excited state has no longer four equivalent minima at α = 0, 90, 180 and 270° as in the ground state. Given $\nu_{body} < \nu_{hat}$, the interaction potential in eqn (2a) has two equivalent absolute minima at α = 0 and 180° and two equivalent secondary minima at α = 90 and 270°. Note that the absolute and secondary minima are exchanged in eqn (2b). Accordingly, the large amplitude motion along the tunneling coordinate connects minima of same depth for $\Delta\alpha$ = 180° in the vibrationally excited dimer instead of $\Delta\alpha$ = 90° in the ground state dimer. The splitting due to tunneling is therefore much smaller in the vibrationally excited dimer.

When replacing α by α + 90°, *i.e.* when exchanging the role of the indiscernable acetylene moieties, H_a is transformed into H_b. As a result, when solving the Schrödinger equations built on the Hamiltonians (2a) and (2b), two identical sets of levels are obtained, a degeneracy which is lifted when taking into account the coupling which allows the two C_2H_2 moieties to exchange vibrational excitation. Ref. 15 and 16 have shown that this coupling is small, although it leads to measurable effects when high resolution spectroscopy is performed on the free $(C_2H_2)_2$ dimer. In the present case, a quick look to Fig. 2 shows that the bands assigned to the dimer are quite broad and do not necessitate such a refined treatment. Hence, the coupling which lifts this degeneracy is ignored and only eqn (2a) is considered.

As above for the ground state Hamiltonian, the excited state Hamiltonian H_a (eqn (2a)) is diagonalized after the excited state wavefunction $|\phi_e\rangle$ is expanded over the basis $\sqrt{\frac{1}{2\pi}}\exp(\imath m\alpha)$, $|m|$ being an integer $\leq$26. For simplicity, the dynamical effect of the helium environment on the movement described by this Schrödinger equation is modeled using the same effective rotational constant $b^{He}_{C_2H_2}$ as above when treating of the ground state dimer. The top panel of Fig. 4 shows the corresponding results for the first three states in each tunneling symmetry A, B and E.

Step (iii) absorption spectrum – the absorption spectrum corresponding to excitation of the ν_3 antisymmetric stretch of the C_2H_2 moieties in the dimer stems from transitions between the levels found at steps (i) and (ii) above. Calling $|\phi_g\rangle$ (resp. $|\phi_e\rangle$) the wavefunction of one of these levels in the ground (resp. excited) vibrational state, the corresponding absorption intensity is proportional to the square of relevant transition dipole moment $|\langle\phi_g|\mu_{body}|\phi_e\rangle|^2$ or $|\langle\phi_g|\mu_{hat}|\phi_e\rangle|^2$ whether the body or the hat of the dimer is excited. In the absence of information in the literature, the same magnitude is assumed for μ_{body} and μ_{hat}.

The full absorption spectrum is simulated by including each transition with non zero oscillator strength into PGOPHER, a general program suite for simulating rotational, vibrational and electronic spectra.[25] Those tools dedicated to simulate the ro-vibrational absorption spectra of semirigid asymmetric top molecules are used here under the A reduced form. Each tunneling isomer is treated as a different asymmetric top molecule, populated with its statistical weight (1, 1 and 2 for the isomers of A, B and E symmetry, respectively).

4.3 Input parameters into PGOPHER

The parameters which serve as input into the PGOPHER simulation are transition energies, transition moments, rotational and centrifugal distortion constants. The transition energies and transition moments are obtained as explained at step (iii) of Section 4.2.

Concerning the rotational and centrifugal distortion constants, we could have used the set provided by Fraser *et al.*[15] or the improved one proposed by Didriche *et al.*[19] However, the purpose of these sets was to account for numerous lines measured with an excellent resolution of 10^{-5} cm^{-1} with the rotational quantum numbers J'' and J' as large as 10. The situation is entirely different here. First, the low droplet temperature (0.38 K) limits the transitions which have a significant contribution to those starting from K_a'' = 0, 1 and $J'' \leq 4$. Second the width of the bands attributed to the dimer in Fig. 2 do not necessitate accuracies better than 5×10^{-2} cm^{-1} on the transition energies. Third, when simulating the spectrum of the droplet experiment, it will be convenient to have as few parameters to fit as possible. We thus used a very limited set of rotational and centrifugal distortion constant as input into the PGOPHER simulation: (i) the same set of rotational constants is assigned to the three tunneling isomers, both in their ground and excited vibrational state; (ii) the centrifugal distortion is limited to Δ_K; (iii) the largest rotational constant A of each isomer is identified to the rotational constant $b_{C_2H_2}$ of C_2H_2 that is used at steps (i) and (ii) to determine the relative energies of the tunneling isomers (this implicitly assumes that the shape of the two C_2H_2 moieties of the dimer is not affected by dimerization); (iv) since the rotational constants B and C should be close to each other as in the isolated dimer, they are replaced by their average $\frac{B+C}{2}$.

4.4 Reliability of the simulation procedure

To check the reliability of the simulation procedure detailed in Section 4.2 and to check that the choice of simulation parameters done in the above paragraph is adequate, we used them to determine the transition energies observed by Fraser *et al.* in the absorption spectrum of the free dimer.[15] The comparison between the present calculation and the experimental results of Fraser *et al.* (when available) is shown in Table 3. It carries specifically on transitions which would have a significant weight in the helium droplet environment at 0.38 K. The transitions are labeled by the asymmetric top quantum numbers $J''K_a''K_c''$ and $J'K_a'K_c'$ for the ground and excited vibrational states, respectively. They are of type b. A satisfactory agreement is observed, within 0.035, 0.023 and 0.020 cm^{-1} for the E^+, A_1^+ and B_1^+ levels respectively. We did the same comparison for the body excitation (a-type transitions). It is not shown here but the agreement with the measurements of Fraser *et al.* is even better: 0.0064, 0.0068 and 0.0065 for these three states, respectively.

Given the width of the bands attributed to the dimer in Fig. 2, it is enough to predict their transition energy within a

Table 2 Tunneling barrier (V_4) and spectroscopic constants (in cm^{-1}) used to describe the C–H stretching excitation of the $(C_2H_2)_2$ dimers. (a) Adapted from Fraser *et al.*[15]

	Isolated (a)	He-Droplet (present work)
V_4	33.2	33.2
ν_{body}	3272.328	3271.03 ± 0.02
ν_{hat}	3281.069	3281.37 ± 0.02
$A = b_{C_2H_2}$	1.177	0.95± 0.01
$\frac{B+C}{2}$	0.062	0.04± 0.01
Δ_K	0	0.03± 0.01

5×10^{-2} cm^{-1} accuracy. The agreement that has just been discussed in Table 3 justifies the present approximations, in particular that a very small number of spectroscopic constants serve as inputs into the PGOPHER simulation.

4.5 Simulation of the spectrum taken in the helium droplet environment

The full simulated spectrum is obtained by summing in the proper proportions the contribution of droplets carrying a single C_2H_2 molecule, using the parameters listed in Table 1 and that of droplets carrying a dimer, using the parameters listed in the third column of Table 2. The latter parameters were adjusted by hand so the simulated spectrum best fits the experimental one. The simulated spectrum is shown as a full red curve in Fig. 5 where it is compared to the experimental spectrum. A satisfactory agreement is observed. Nevertheless, two points must be mentioned. First, the simulation and experiment do not agree well in the blue foothill of the P(1) and R(1) lines of acetylene (top left and top right panels of the figure). Second, the calculation predicts combination lines (top right panel of the figure) where the tunneling quantum number changes in addition to the excitation of one acetylene moiety. They are very weak and not observed experimentally, because of the unfavorable signal/noise ratio.

5 Discussion

The discussion examines first how the effective constants used in the simulation are sensitive to specific features of the absorption spectrum. The remaining discussion addresses the information brought by these constants on the effect of the helium environment on the rotation and deformation of $(C_2H_2)_2$.

5.1 Sensitivity of the effective constants to details of the absorption spectrum

The hat excitation of $(C_2H_2)_2$ is considered first. It is characterized by a well-resolved triplet structure: the K_a-triplet, whose components are labeled $K_a(0 \leftarrow 1)$, $K_a(1 \leftarrow 0)$ and $K_a(2 \leftarrow 1)$ in Fig. 5. The key constants to adjust for reproducing this structure in the simulated spectrum are the rotational constant A^{He}, the centrifugal distortion constant Δ_K^{He} and the band origin ν_{hat}^{He}. A^{He} and Δ_K^{He} act on the spacing between the three sub-bands, whereas the overall location of the triplet is essentially determined by ν_{hat}^{He}. Note that the calculation of the tunneling isomers and the fit to the experimental data were performed iteratively in a self-consistent way in order to maintain the equality $A^{He} = b_{C_2H_2}^{He}$.

Table 3 Comparison between the measurements of Fraser *et al.*[15] and the present calculations for transitions corresponding to the hat excitation of the free $(C_2H_2)_2$ dimer (energies in cm^{-1}). The comparison is limited to the lines which have a significant intensity when running the simulation at 0.38 K. The $K_a' = 2 \leftarrow K_a'' = 1$ transitions were not reported by Fraser *et al.* and are not included in the table. (a) Fraser *et al.*[15] (b) Present work

J'	K_a'	K_c'	J''	K_a''	K_c''	E^+	A_1^+	B_1^+	Ref.
1	1	1	0	0	0	3282.0471	3282.0783	...	(a)
						3281.9677	3282.0027	3281.9287	(b)
2	1	2	1	0	1	3282.1558	...	3282.1136	(a)
						3282.0915	3282.1265	3282.0525	(b)
1	1	1	2	0	2	3281.6757	3281.7068	...	(a)
						3281.5963	3281.6313	3281.5573	(b)
3	1	3	2	0	2	3282.2877	3282.3168	...	(a)
						3282.2153	3282.2503	3282.1763	(b)
2	1	2	3	0	3	3281.5367	...	3281.4949	(a)
						3281.4725	3281.5075	3281.4335	(b)
4	1	4	3	0	3	3282.4000	...	3282.3515	(a)
						3282.3391	3282.3741	3282.3001	(b)
1	0	1	1	1	0	3279.5945	3279.6482	3279.5616	(a)
						3279.6142	3279.6504	3279.5572	(b)
0	0	0	1	1	1	3279.4755	3279.5281	3279.4418	(a)
						3279.4904	3279.5252	3279.4512	(b)
2	0	2	1	1	1	3279.8445	3279.8996	3279.8150	(a)
						3279.8618	3279.8966	3279.8226	(b)
2	0	2	2	1	1	3279.5898	3279.6445	3279.5578	(a)
						3279.6145	3279.6507	3279.5750	(b)
3	0	3	2	1	2	3279.9727	3280.0294	3279.9441	(a)
						3279.9778	3280.0204	3279.9464	(b)
3	0	3	3	1	2	3279.5845	3279.6410	3279.5563	(a)
						3279.6150	3279.6490	3279.5750	(b)
1	0	1	2	1	2	3279.3548	3279.4085	3279.3219	(a)
						3279.3669	3279.4031	3279.3274	(b)
2	0	2	3	1	3	3279.2360	3279.2908	3279.2066	(a)
						3279.2436	3279.2776	3279.2036	(b)
4	0	4	3	1	3	3280.1060	3280.1587	3280.0715	(a)
						3280.1103	3280.1443	3280.0703	(b)
4	0	4	4	1	3	3279.5809	3279.6334	...	(a)
						3279.6157	3279.6490	3279.5750	(b)
3	0	3	4	1	4	3279.1205	3279.1771	3279.0920	(a)
						3279.1205	3279.1538	3279.0798	(b)

From Section 4.2 we know that the dimer is modeled as three distinct asymmetric top molecules, one for each tunneling isomer. Each leads to a distinct K_a-triplet. The simulation shows that each sub-bands of the triplets moves by less than 0.06 cm^{-1} when switching from one isomer to the other. Hence, when summing the contribution of the three isomers to build the full spectrum, the shape and width of the K_a sub-bands are not dramatically affected by the existence of these isomers. Nevertheless, the tunneling isomers play a subtle role. The K_a sub-bands appear with no sub-structure because they are the superposition of lines associated with the slow overall rotation of the dimer within the droplet, slightly displaced when switching from one isomer to the other. As a result, the width of the unstructured K_a sub-band documents the slow rotation, essentially. It is described by the effective constant $\left.\frac{B+C}{2}\right|^{He}$, which is therefore fairly sensitively determined when fitting the width of the unstructured K_a sub-bands in the simulation. Including the tunneling also affects the shape of the K_a sub-bands because

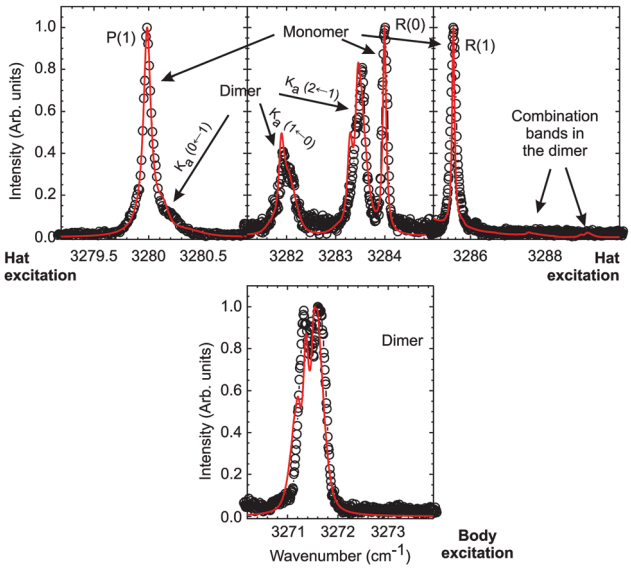

Fig. 5 Comparison between the simulated (full red curve) spectrum and the experimental (open circle) one taken from Fig. 2. The three top panels show the important spectral regions of the hat excitation and the bottom panel that of the body excitation. The peak of largest intensity is normalized to one in each panel.

the nuclear spin statistics does not appear in the same way whether it is included or not. It appears within the 1A + 1B + 2E summation in the first case and is given by the 3 : 1 statistics ($3A_1$+ $1B_2$) in the second case.

The lower panel of Fig. 5 shows the body excitation of the dimer. The corresponding transition moment is parallel to the symmetry axis of the T-shaped dimer. This transition is very congested since it has no well resolved K_a structure. This band is therefore of very poor help for fitting the effective constants A^{He}, Δ_K^{He} and $\left.\frac{B+C}{2}\right|^{He}$, which rely essentially on the fit to the K_a-triplet in the hat excitation. Only the band origin ν_{body}^{He} is sensitively determined when fitting the body excitation.

5.2 Rotational and centrifugal distortion constants A^{He} and Δ_K^{He}

Table 2 shows that constant A^{He} is reduced by 22% in the droplet experiment, whereas Δ_K^{He} is enhanced drastically, switching from zero for the free dimer to 0.03 cm^{-1} in the droplet experiment. Introducing such a large effective value is absolutely necessary to reproduce the spacing between the bands labeled $K_a(1 \leftarrow 0)$ and $K_a(2 \leftarrow 1)$ in Fig. 5 after the rotational constant A is determined for a correct spacing between the bands $K_a(0 \leftarrow 1)$ and $K_a(1 \leftarrow 0)$.

Actually, the constants A^{He} and Δ_K^{He} play a similar role when fitting the dimer data than the constants B^{He} and D^{He} when fitting the monomer data. In the latter case indeed, the spacing between the P(1) and R(0) bands of the monomer is equal to $4B$–$4D$ whereas that between R(0) and R(1) is $4B$–$32D$, hence the large value of D^{He} allows the R(1) band to be at the right distance from R(0), otherwise its separation from R(0) would be too large by 0.5 cm^{-1}.

The effective values of B^{He} and D^{He} in the droplet environment were discussed by Nauta and Miller[11] and interpreted quantitatively by Zillich *et al.*[8] It appears that the rotational levels of $J = 0$ and 1 of C_2H_2 are only weakly perturbed by the droplet, whereas the $J = 2$ level is significantly perturbed and displaced to low energies by a strong direct coupling to the roton and maxon excitations of the droplet. This picture likely applies to the T-shaped $(C_2H_2)_2$ dimer when the body is the rotation axis. In a near symmetric top picture of the dimer, this rotation is described by the projection K_a of the total angular momentum along the body of the dimer. The three bands labeled $K_a(0 \leftarrow 1)$, $K_a(1 \leftarrow 0)$ and $K_a(2 \leftarrow 1)$ for the dimer in Fig. 5 can be identified to the P(1), R(0) and R(1) transitions of the monomer. Similarly, the effective rotational constant A^{He} (resp. the effective centrifugal distortion constant Δ_K^{He}) of the dimer plays the same role as the effective B^{He} (resp. effective D^{He}) constant of the monomer.

An interesting observation is done when comparing Tables 1 and 2: the rotational constant A^{He} of the dimer about its symmetry axis is significantly smaller than the rotational constant B^{He} of the acetylene monomer (0.95 *versus* 1.04 cm^{-1}); moreover, Δ_K^{He} for the dimer is substantially larger than D^{He} for the monomer (0.03 *versus* 0.019 cm^{-1}). These two observations suggest that the rotation of the acetylene dimer is more strongly coupled to the helium environment than that of the monomer: the smaller effective value of A^{He} suggests that the non-superfluid component of the droplet is more driven into rotation by the dimer than by the monomer; the non-superfluid component may also have a larger extension when solvating the dimer; larger effective value of Δ_K suggest that the $K_a = 2$ rotational states of the dimer are more coupled than the $J = 2$ rotational state of the monomer with the roton and maxon excitation of the superfluid component of the droplet. Both effects are consistent since a more rapid rotation of the non-superfluid component or a larger extension of this component can stimulate more efficiently the coupling with the collective roton/maxon excitation of the outer superfluid component.

This conclusion is somehow puzzling when brought together with our previous work on the Ne–C_2H_2 complex.[10] The latter work compares the effective rotational and centrifugal distortion constants B^{He} and D^{He} for the C_2H_2 monomer with those of the Ne–C_2H_2 complex and concludes that the presence of Ne facilitates the slow rotation of C_2H_2 ($J = 1$) and leaves unaffected the coupling of $J = 2$ with the roton/maxon excitation. The situation here with the $(C_2H_2)_2$ dimer is actually not fully comparable with that of the Ne–C_2H_2 complex. The rotation of C_2H_2 in Ne–C_2H_2 is indeed quasi free, *i.e.* it can proceed freely about two axis perpendicular to the C_2H_2 symmetry axis, whereas in the $(C_2H_2)_2$ dimer, the rotation of C_2H_2 is hindered along the tunneling axis α and free on the other. This certainly affects the rotation dynamics of the dimer, which is coupled to the superfluid and non-superfluid component of the droplet.

Douberly *et al.* have reported the infrared spectrum of the C_2H_2–HF complex in helium droplets. The complex is T-shaped with the H atom of HF pointing towards the C≡C triple bond

of C_2H_2.[26] Exciting the C–H antisymmetric stretch in this complex is thus comparable to the present hat excitation of $(C_2H_2)_2$. Interestingly, the effective rotational constant A which is measured by these authors for the complex is very close to that given in Table 2 for $(C_2H_2)_2$ ($A' = A'' = 0.9679$ cm^{-1} in ref. 26 *versus* $A^{He} = 0.95$ cm^{-1} here). The effective centrifugal distorsion constant Δ_K is also similar in both work ($\Delta_K' = 0.0182$ cm^{-1} in ref. 26 *versus* $\Delta_K^{He} = 0.019$ cm^{-1} here). This indicates that the excitation of the hat in $(C_2H_2)_2$ and that of the C_2H_2 moiety in C_2H_2–HF are coupled in a similar way to the superfluid and non-superfluid components of the droplet.

5.3 Rotational constants A^{He} and $\left.\frac{B+C}{2}\right|^{He}$

The comparison between the constants A^{He} and $\left.\frac{B+C}{2}\right|^{He}$ and their counterpart in the free dimer is qualitatively consistent with the picture recalled at several points in this paper: the non-superfluid component of the droplet is more likely to follow adiabatically slow than rapid rotations. When considering the rapid rotation about the body of the dimer, the ratio $A:A^{He}$ = 1.23 is actually close to 1 as expected when the non-superfluid component is badly driven into rotation by the molecular rotation. The ratio $\frac{B+C}{2}:\left.\frac{B+C}{2}\right|^{He}$ documents the much slower rotation about the rotation axis which are perpendicular to the body. An adiabatic following of molecular rotation by the non-superfluid component is expected in this case and actually the $\frac{B+C}{2}:\left.\frac{B+C}{2}\right|^{He} = 1.5$ is larger than $A:A^{He}$ = 1.23. Nevertheless, a much larger value of 3 or more would be expected for such a slow rotation.[3] This apparent contradiction is due to the fact that slow rotation described by the $\frac{B+C}{2}$ is always mixed with the rapid rotation about the body of dimer, either in the ground or in the excited vibrational state or both. Whatever the transition which is considered, K_a' or K_a'' is non-zero. The coupling with the non-superfluid component of the droplet is therefore very different than encountered when only the slow rotation of an heavy rotor is present.

The fact that the effective rotational constant associated with a slow rotation is not as small compared to the gas phase value than expected has already been encountered for a symmetric top molecule, C_2H_6, that Gomez *et al.* observed in infrared range near 3 μm in helium droplets.[27] The effective rotational constant B is only a factor 2.04 smaller than the gas phase value (0.325 *versus* 0.663 cm^{-1}). The situation is somehow comparable to the present one. Because of the exchange property of the nuclear spin of the H-atoms in C_2H_6, a fraction of the ground vibrational state molecules have necessarily a non-zero projection of the angular momentum about the symmetry axis of the molecule. These molecules make a rapid rotation about this axis, which is superimposed to the slow rotation about the two other axis.

Let us recall once more the work of Douberly *et al.* on the C_2H_2–HF complex in helium droplets.[26] It is striking to notice that the value $\frac{B''+C''}{2} \approx \frac{B'+C'}{2} = 0.06872$ cm^{-1} found for the C_2H_2–HF complex is very close to the present value of 0.06 cm^{-1} given to $\left.\frac{B+C}{2}\right|^{He}$ in Table 2.

5.4 Band origins ν_{hat}^{He} and ν_{body}^{He}

Both the observations of Nauta and Miller and those of Briant *et al.* show that the excitation of the C–H antisymmetric stretch in the C_2H_2 monomer has effective band origins ν_{LD} and ν_{UD} in helium droplets that are very slightly blue shifted with respect to their value when C_2H_2 is isolated (0.127 and 0.129 cm^{-1}, respectively in ref. 11; 0.089 and 0.149 cm^{-1} in ref. 10). A similar behaviour is observed here with the hat excitation. The effective band origin $\nu_{hat}^{He} = 3281.37$ cm^{-1} is blue shifted by 0.30 cm^{-1} with respect to the value measured in ref. 15 when $(C_2H_2)_2$ is isolated. The observation of a 1.30 cm^{-1} red shift for ν_{body}^{He} is therefore unexpected.

This observation must be brought together with the band origins of the HF and H–CC–H stretches which are documented by Douberly *et al.*[26] The C_2H_2–HF complex is T-shaped with HCCH in the hat position, attracting the H atom of HF. HF thus occupies the body location in the C_2H_2–HF complex. The band origin of the antisymmetric H–CC–H stretch of C_2H_2–HF is slightly blue shifted by 0.0784 cm^{-1}, in the droplet compared to the situation where the complex is isolated. In contrast, a large red shift of 6.869 cm^{-1} is reported by Douberly *et al.* in the helium droplets for the HF stretch. This strikingly mimics the present results for the hat and body excitation of the $(C_2H_2)_2$ dimer. Similar observations were done in other H-bonded complexes.[28,29] Focusing their attention to the large red shift of the body excitation, Douberly *et al.* proposed that the helium density around the hydrogen bond could be quite high since helium is attracted both by the F end of HF and the CC core of C_2H_2. Such a picture is easy to transpose to the present $(C_2H_2)_2$ dimer. A non-spherical repartition of helium about the acetylene dimer may indeed influence the molecular vibration differently whether a or b transitions are concerned.

6 Summary and conclusion

The acetylene dimer $(C_2H_2)_2$ was formed by picking up C_2H_2 molecules in helium droplets constituted of a few thousand atoms. The antisymmetric CH stretch of the two acetylene moieties of the dimer were studied by infrared absorption spectroscopy according to the helium nanodroplet isolation technique (HENDI). The spectral region between 3270 and 3290 cm^{-1} was explored. The experimental observations were interpreted on the basis of simulations of the absorption spectrum. The later takes into account the tunneling behavior due to the geared contra rotatory motion of the acetylene moieties, which exchange their role in the T-shaped dimer.

The simulation served to derive effective spectroscopic constants for the dimer by fitting the experimental spectrum. A very small number of constants were included in the fit,

namely the band origins of the C–H excitation for the hat and the body of the T-shaped dimer and, following an asymmetric top description of the tunneling isomers of the dimer, the rotational constants A and $\frac{B+C}{2}$ and the centrifugal distortion constant Δ_K. It was very instructive to compare these effective spectroscopic constants to their equivalent for the C_2H_2 monomer, the HF–C_2H_2 complex and the C_2H_6 symmetric top molecule, which are available in the literature. This allowed us to draw general trends for the dynamical role played by the helium environment on a floppy molecular assembly which is excited both vibrationally and rotationally by a laser.

Although one aim of the paper was to examine how the helium environment affects the tunneling motion which exchanges the role of the acetylene moieties in the dimer, no salient feature of the absorption spectrum could be associated with this motion. In contrast, quite subtle effects of the helium dynamics where observed on the rotations of the dimer and on vibrational excitation of the two acetylene moieties. All of them were rationalized by suggesting that the non-superfluid component of the droplet has a larger extension or is more adiabatically coupled to the rotating dimer than observed with the C_2H_2 monomer or the C_2H_2–Ne complex. Importantly, a strong parallel could be done between the present observation of the C_2H_2–C_2H_2 dimer and the observations of Douberly *et al.* on the C_2H_2–HF complex. Both are T-shaped and C_2H_2 forms the hat of C_2H_2–HF. It appears that the hat of both complexes are coupled to the molecular environment in a quantitatively similar way. When comparing the effective constants for the slow rotation about the axis perpendicular to the body of these complexes, the coupling of the helium atoms to the global molecular rotation is only qualitatively accounted by the simple picture where slow rotations are followed adiabatically by the non-superfluid component of the droplet. Finally, the comparison between the C_2H_2–C_2H_2 and C_2H_2–HF complexes suggests that in both cases, the helium distribution and density about them is in situation to red shift the vibrational excitation of the body of the complex by more than 1 cm^{-1}, whereas the hat excitation is only marginally affected. This highlights that in spite of its superfluid character, the helium droplet has a non-trivial effect on rotation, deformation and vibrational excitation of hosted molecular assemblies. In our opinion, this should motivate extensive theoretical approaches to model the dynamics of floppy molecular assemblies within a quantum fluid.

Conflicts of interest

There are no conflicts to declare.

Acknowledgements

This work was supported partly by Agence Nationale de la Recherche under Grant ESBODYR ANR-14-CE06-0019 and by ''Investissements d'Avenir'' LabEx PALM (ANR-10-LABX-0039-PALM). E. M. acknowledges support by Eurotalent under Grant 2015#259.

References

1 M. Hartmann, F. Mielke, J. P. Toennies, A. F. Vilesov and G. Benedek, *Phys. Rev. Lett.*, 1996, **76**, 4560–4563.
2 F. Stienkemeier, W. E. Ernst, J. Higgins and G. Scoles, *J. Chem. Phys.*, 1995, **102**, 615–617.
3 C. Callegari, K. K. Lehmann, R. Schmied and G. Scoles, *J. Chem. Phys.*, 2001, **115**, 10090–10110.
4 J. P. Toennies, A. F. Vilesov and K. B. Whaley, *Phys. Today*, 2001, **54**, 31–37.
5 M. Y. Choi, G. E. Douberly, T. M. Falconer, W. K. Lewis, C. M. Lindsay, J. M. Merritt, P. L. Stiles and R. E. Miller, *Int. Rev. Phys. Chem.*, 2006, **25**, 15–75.
6 J. P. Toennies, *Mol. Phys.*, 2013, **111**, 1879–1891.
7 Y. Kwon, P. Huang, M. V. Patel, D. Blume and K. B. Whaley, *J. Chem. Phys.*, 2000, **113**, 6469–6501.
8 R. E. Zillich, Y. Kwon and K. B. Whaley, *Phys. Rev. Lett.*, 2004, **93**, 250401.
9 R. E. Zillich, F. Paesani, Y. Kwon and K. B. Whaley, *J. Chem. Phys.*, 2005, **123**, 114301.
10 M. Briant, E. Mengesha, P. de Pujo, M.-A. Gaveau, B. Soep, J.-M. Mestdagh and L. Poisson, *Phys. Chem. Chem. Phys.*, 2016, **18**, 16414–16422.
11 K. Nauta and R. E. Miller, *J. Chem. Phys.*, 2001, **115**, 8384–8392.
12 A. Metzelthin, O. Birer, E. Sanchez-Garcia and M. Havenith, *J. Chem. Phys.*, 2008, **129**, 114307.
13 R. D. Pendley and G. E. Ewing, *J. Chem. Phys.*, 1983, **78**, 3531–3540.
14 D. G. Prichard, R. N. Nandi and J. S. Muenter, *J. Chem. Phys.*, 1988, **89**, 115–123.
15 G. T. Fraser, R. D. Suenram, F. J. Lovas, A. S. Pine, J. T. Hougen, W. J. Lafferty and J. S. Muenter, *J. Chem. Phys.*, 1988, **89**, 6028–6045.
16 G. T. Fraser, *J. Chem. Phys.*, 1989, **90**, 2097–2108.
17 Y. Ohshima, Y. Matsumoto, M. Takami and K. Kuchitsu, *Chem. Phys. Lett.*, 1988, **147**, 1–6.
18 Y. Ohshima, Y. Matsumoto, M. Takami and K. Kuchitsu, *Chem. Phys. Lett.*, 1988, **152**, 116–117.
19 K. Didriche, C. Lauzin, T. Foldes, D. Golebiowski, M. Herman and C. Leforestier, *Phys. Chem. Chem. Phys.*, 2011, **13**, 14010–14018.
20 C. Leforestier, A. Tekin, G. Jansen and M. Herman, *J. Chem. Phys.*, 2011, **135**, 234306.
21 U. Buck, *Molecular Scattering; Physical and Chemical Applications*, Wiley, Chichester, Sussex, England, 1975, pp. 313–388.
22 O. Bunermann and F. Stienkemeier, *Eur. Phys. J. D*, 2011, **61**, 645–655.
23 J.-M. Mestdagh, M.-A. Gaveau, C. Gée, O. Sublemontier and J. P. Visticot, *Int. Rev. Phys. Chem.*, 1997, **16**, 215–247.
24 S. van der Walt, S. Colbert and G. Varoquaux, *Comput. Sci. Eng.*, 2011, **13**, 22–30.
25 C. M. Western, *PGOPHER, a Program for Simulating Rotational Structure*, 2013.
26 G. E. Douberly, K. Nauta and R. E. Miller, *Chem. Phys. Lett.*, 2003, **377**, 384–390.
27 L. F. Gomez, R. Sliter, D. Skvortsov, H. Hoshina, G. E. Douberly and A. F. Vilesov, *J. Phys. Chem. A*, 2013, **117**, 13648–13653.
28 K. Nauta and R. E. Miller, *J. Chem. Phys.*, 1999, **111**, 3426–3433.
29 K. Nauta and R. E. Miller, *Chem. Phys. Lett.*, 2001, **346**, 129–134.